Review

Oxidation Kinetics of FeCr and FeCrAl Alloys: Influence of Secondary Processes

Irakli Nakhutsrishvil *

Posted Date: 19 September 2023

doi: 10.20944/preprints202309.1173.v1

Keywords: Metal/alloy oxidation kinetics; scale evaporation; change of reaction area

Review

Oxidation Kinetics of FeCr and FeCrAl Alloys: Influence of Secondary Processes (mini review)

Irakli Nakhutsrishvili

Institute of Cybernetics, Georgian Technical University

Abstract: The work presents a mathematical model of a thermogravimetric curve for the growth and simultaneous sublimation of scale on a metal or alloy surface. Reduction of the reaction area as a result of the formation of oxides of alloying elements (for obtaining the basic oxide) is considered for the alloy. For metals, the case where this area is increased as a result of powder metal crushing is also considered. The equations that were obtained are employed to explain the kinetic curves of the mass change of the samples.

Keywords: Metal/alloy oxidation kinetics; scale evaporation; change of reaction area

1. Introduction

Scale growth on the surface of a metal or alloy is often accompanied by secondary processes that limit the kinetics of the process. Scale can partially sublimate, it is also possible to change the reaction surface for the growth of the main oxide. These processes - separately or together - lead to a significant change the form of equations used to describe the kinetics of the interaction of active gases with the surface of solids.

In the absence of secondary processes, the kinetics of scale growth on the surface of a metal or alloy is parabolic. In some cases, subparabolic, cubic and quaternary processes are also realized. In general: $m^n=k_nt$ or (in differential form)

$$dm/dt = k_n/nm^{n-1}, \quad (1)$$

where m is a specific mass gain of oxidized object over time t (mass change due to reacted oxigen), k_n is the reaction constant, n = 2, 3, 4 and can also take fractional values.

From Eq.(1) it follows an infinite initial value $dm/dt=\infty$ (at the origin: t=0, m=0). To eliminate this infinity, instead of a simple parabolic equation, a "complex" equation $(m/k_r)+(m^2/k_p)=t$ qan be used, where k_r is rectilinear constant (dm/dt at the origin). In this case we will have:

$$dm/dt=\frac{k_n/n}{m^{n-1}+k_n/nk_r}. \quad (2)$$

In particular, for parabilic kinetic:

$$dm/dt=\frac{kp}{2m+kp/kr} \quad (3)$$

Chromium-based alloys (alumina and chromium-forming alloys) are materials for coating hot parts of gas turbine and jet engines, solar power plants, etc. These alloys have been studied both earlier [1,2] and recently [3,4]. During the oxidation of these alloys, Al_2O_3 or Cr_2O_3 scale is formed on their surface. To improve the adhesion of the scale, doping of the alloy with rare earth metals (REM: La, Y, Ce etc.) is used [5-8], as for other alloys [9-13].

In this case, fine particles of perovskites are formed - compounds of the RMO_3 type, where R is a rare earth element, and M is one of the two (three) main components of the alloy. The boundaries of oxide grains (the main arteries of mass transfer) in it are blocked by diffusion barriers made of chromites ($LaCrO_3$, $YCrO_3$, $CeCrO_3$). Having close-packed sublattices, these particles are barriers to cation diffusion. This leads to a significant change in the oxidation kinetics (in contrast to the usual parabolic). U.R. Evans [14] defined reduction of surface (S) as:

$$dS/dm=-kS \quad (4)$$

or (in integral form):

Preprints (www.preprints.org) | NOT PEER-REVIEWED | Posted: 19 September 2023 doi:10.20944/preprints202309.1173.v1

$$S=S_0e^{-km}, \quad (5)$$

where k is a constant of reduction of the reaction area, and S_0 is the initial size. Taking into account that in the absence of a change in the effective area (k=0), the scale growth occurs according to the parabolic law

$$m^2=k_pt \quad (6)$$

k_p - parabolic constant, t - time). From Eqs(3-6):

$$dm/dt=(k_p/2m)e^{km}. \quad (7)$$

The solution to Eq.(7) is the implicit expression (boundary conditions t=0, m=0):

$$t=2(k^2k_p)^{-1}[e^{km}(km-1)+1]. \quad (8)$$

By using of ''complex'' parabola we will have:

$$dm/dt = k_pe^{-km}/(2m+k_p/k_r) \quad (9)$$

and

$$t=2(k^2k_p)^{-1}[e^{km}(km-1)+1]+(kk_r)^{-1}(e^{km}-1). \quad (10)$$

It can be seen that for $k_r\rightarrow\infty$ Eq.(9) goes over to Eq.(8).

By combining of Eq.(5) with Eqs (8) and (10) we can write:

$$t=[2(kk_p)^{-1}][1-\varphi^{-1}\ln(e\varphi)], \quad (11)$$

$$t=[2(kk_p)^{-1}][1-\varphi^{-1}\ln(e\varphi)]+(kk_r)^{-1}(\varphi^{-1}-1), \quad (12)$$

where $\varphi=S/S_0$.

The above equations are used in subsequent sections to describe the kinetics of high-temperature oxidation in air of FeCr and FeCrAl alloys doped with La.

The results obtained in [15-17] are combined in this paper. The following experimental data for FeCrAl differ from [17], since the experiment was carried out at a different temperature.

2. Results and Discussion

2.1. Oxidation of alloy Fe44Cr4Al0.25La at 1300°C

There are a large number of publications devoted to the study of high-temperature oxidation of FeCrAl alloys. In this case, a protective film of aluminum oxide is formed [18-15]. When using lanthanum, to improve of film adhesion and mechanical properties of the alloy, the formation of non-basic oxides and aluminates (in particular $LaAlO_3$) occurs [26,27]. As mentioned above, this phase belongs to perovskites [28,29] and is diffusely impermeable. During the oxidation of FeCr, FeCrAl, FeCrAl(REM) and other similar reactions, a parabolic, sub-parabilic or cubic law of kinetics is observed [30-38].

In this section, the process of oxidation of Fe44Cr4Al0.3La (wt.%) in air at 1300°C is considered. The resulting experimental curve is presented in Fig.1 (curve 1). In this case, the total mass change M = m. The tangent at the origin gives a high value of k_r. Therefore, equations (8) and (10) can be used ($k_r\rightarrow\infty$). Using the OriginPro8 program to determine other constants, we obtain the following empirical equations:

$$t\cong4.77[e^{1.49m}(1.49m-1)+1] \quad (13)$$

$$t\cong4.77[1-\varphi^{-1}\ln(e\varphi)]. \quad (14)$$

The curves plotted using these expressions are presented in Fig.1.

Preprints (www.preprints.org) | NOT PEER-REVIEWED | Posted: 19 September 2023 doi:10.20944/preprints202309.1173.v1

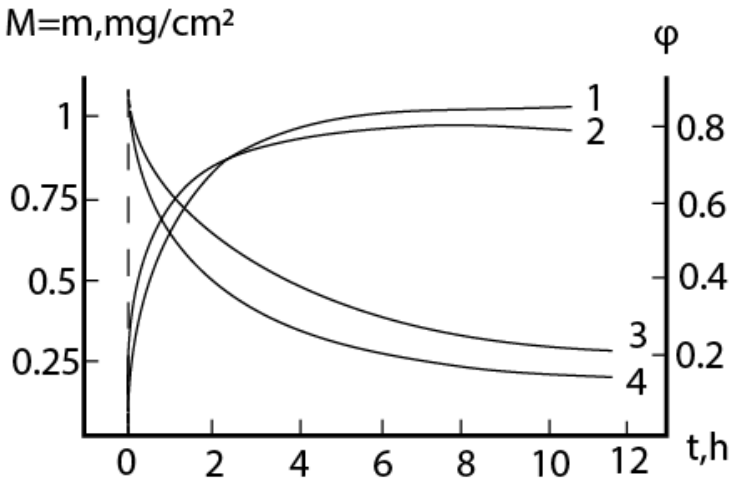

Figure 1. Experimental (1, 3) and calculated (2, 4) curves of mass gain and reduction of φ.

Let's briefly mention the previously established advantages of FeCrAl(La) and other FeCrAl(REM) system alloys [39-41]: relatively less weight, heat capacity, greater stability in aggressive gases, as well as high resistance to mechanical wear as determined by us.

2.2. Oxidation of alloy Fe45Cr0.3La at 1300°C

Lanthanum-doped FeCr alloys have high heat resistance up 1300 to 1400 °C. Similar to alumina-forming alloys, during the oxidation of FeCr(La), along with the main oxide Cr_2O_3, difficult-to-permeate chromite $LaCrO_3$ is formed. At the same time, a characteristic property of Cr_2O_3 is intense evaporation at 1100-1400°C (evaporation of Al_2O_3 requires a higher temperature). In this case, the total mass change is $M = m - v_m t$, where v_m is the evaporation rate of reaction products by the metal component. In this case:

$$dm/dt=\frac{kp}{2m+kp/kr}e^{-km}-v_g \qquad (15)$$

and

$$dM/dt=\frac{kp}{2m+kp/kr}e^{-km}-v_g-v_m=\frac{kp}{2m+kp/kr}e^{-km}-v_p, \qquad (16)$$

where v_g is the evaporation rate of reaction products by the gaseous component, and $v_p=v_g+v_m$. Differential equations (15) and (16) lead to an integral of the form $y=\int \frac{xe^{ax}}{b+cxe^{ax}}dx$, which cannot be represented using elementary functions.

The total mass change can be represented only in the parametric form:

$$M=m-[\frac{2v_m}{k^2k_p}e^{km}(km-1)+1]+\frac{2v_m}{kk_r}(e^{km}-1) \qquad (17)$$

with the parameter $m=M+v_m t$. This means that when constructing the calculated dependences M - t, t is first found by m using Eq.(10), and then, given the same m, M is calculated using $M = m - v_m t$. Consequently, the m - t dependence can be constructed as $m = M + v_m t$ (Fig.1) (in case of alumina-forming alloy m=M).

According to our data, at 1300°C the evaporation rate of C_2O_3 is $\cong 4 \bullet 10^{-3}$ mg/cm²h, and for $LaCrO_3$ is $\cong 8 \bullet 10^{-4}$ mg/cm²h. Taking this into account, Fig.2, along with experimental curve 1, shows the curve of alloy mass change due to reacted oxygen (curve 2). It can be seen from the figure that the

Preprints (www.preprints.org) | NOT PEER-REVIEWED | Posted: 19 September 2023 doi:10.20944/preprints202309.1173.v1

slope of the tangent to the experimental curve at the origin of coordinates has a real value (in the case of an alumina-forming alloy, the tangent practically coincided with the ordinate axis). In this case, Eqs(10) and (12) must be used in full. Empirical expressions will be:

$$t \cong 6.04[e^{0.59m}(0.59m-1)+1]+0.59(e^{0.59m}-1) \quad (16)$$

and

$$t \cong 6.04[1-\varphi^{-1}\ln(e\varphi)]+0.59(\varphi^{-1}-1), \quad (17)$$

where m is in mg/cm² and t is in hours. The curves plotted using these expressions are presented in Fig.2.

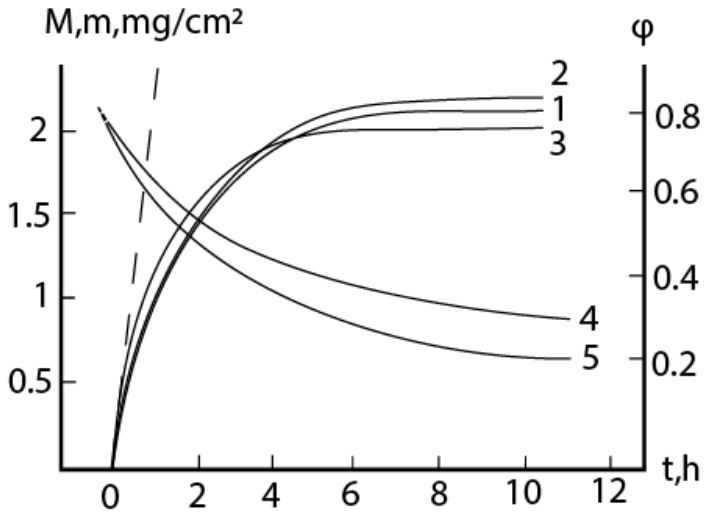

Figure 2. Experimental (1, 4) and calculated (3, 5) curves of mass gain and reduction of φ; 2 – curve of mass change due to reacted oxygen. The dotted line is tangent to the curve at the point t=0,m=0.

FeCr and FeCr(REM), as well as FeCrAl alloys, are widely used in technology both previously and today [42].

2.3. Consideration of initial non-isothermal heating during oxidation of alloys: Oxidation of alloy Fe45Cr0.32Y at 1400°C

In a number of works, the oxidation of alloys was studied under non-isothermal conditions [43-]. A similar situation occurs in isothermal processes, when the operating temperature is reached within a certain time. Figure 3 schematically shows the kinetic curve of such a process: the initial non-isothermal heating lasts for a time t_0, while the mass of the alloy increases by m_0. It is obvious that in the future it is necessary to use a new coordinate system ($m = w-m_0$; $t = t_w-t_0$) with the beginning at the inflection point (from Eqs(9) and (10) it follows that the graphs of mass increase should be convex in the positive direction). The branch of the curve lying in the first quadrant of the new coordinate system can already be described by Eq.(10). A formal mathematical study of this implicit function shows that its graph has a vertex in the third quadrant of the m - t coordinate system with the ordinate $m_{dt/dm=0} \equiv \bar{m}=-k_p/2k_r$ (the corresponding abscissa ($\bar{t}$) can be found by substituting $\bar{m}$ into equation (10)).

Preprints (www.preprints.org) | NOT PEER-REVIEWED | Posted: 19 September 2023 doi:10.20944/preprints202309.1173.v1

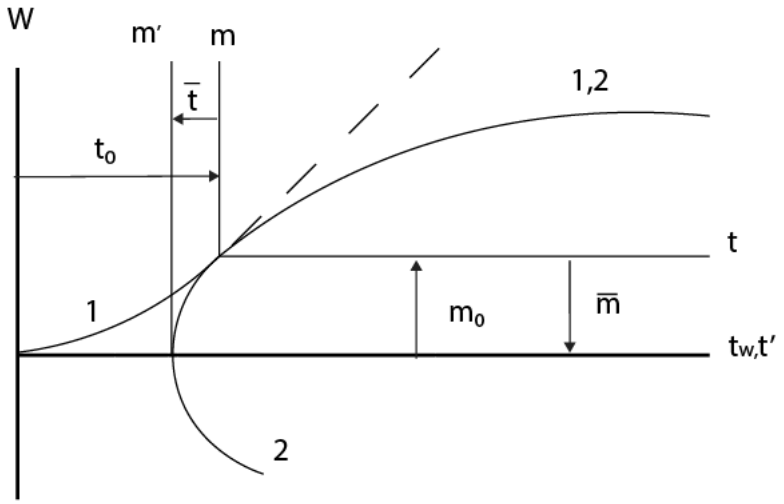

Figure 3. Schematic representations of the complete cycle of mass gain of the alloy - (1) and function (10) - (2). The dotted line is tangent to the curve at the point t=0,m=0.

The curve in Fig. 3 is constructed so that $m_0=-\bar{m}=k_P/2k_r$. However, there is no mathematical justification for the statement that the initial mass gain (m_0) and the ordinate of the peak of the curve ($\bar{m}$) must be equal in absolute value. However, the validity of this relationship was empirically established earlier during relatively slow heating of iron-chromium alloys doped with lanthanum or yttrium [43-46]. Here, heating to the operating temperature occurred at a rate of 24°C/min (in the processes described in sections 2.1 and 2.2, the operating temperature was reached in 2-3 minutes and the effects considered in this section could be ignored).

Shifting the origin of the coordinates again to the point ($\bar{t}$,$\bar{m}$), we can consider the ideal kinetic curve in the coordinate system (m',t'), corresponding to the mass gain of the alloy with the instantaneous achievement of the operating temperature. In these coordinates we can already use Eq.(8).

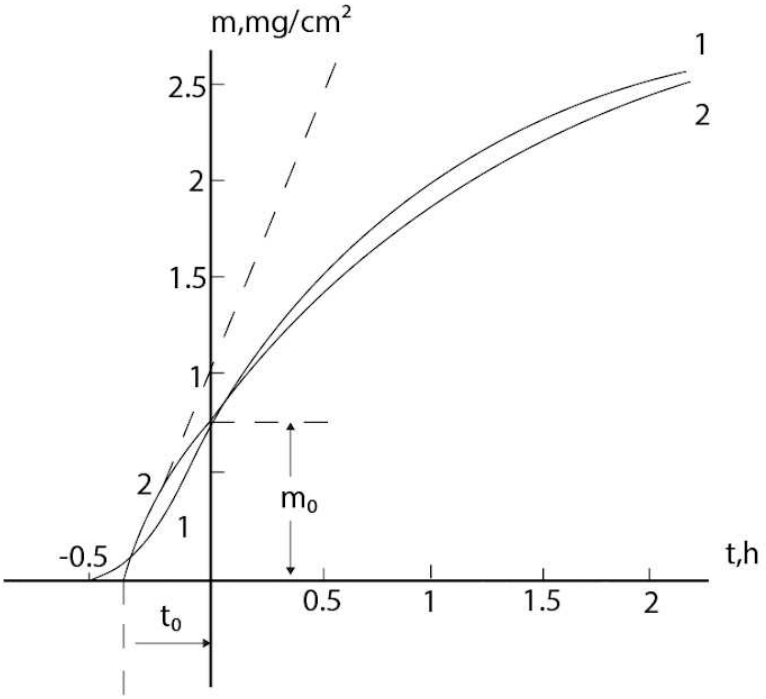

Preprints (www.preprints.org) | NOT PEER-REVIEWED | Posted: 19 September 2023 doi:10.20944/preprints202309.1173.v1

Figure 4. Curve constructed from experimental data taking into account the evaporation of Cr_2O_3 and $YCrO_3$ (1) and calculated curve of mass gain (2).

During the oxidation of FeCr(Y), chromite is also formed - $YCrO_3$ [15,47-51], which creates diffusion barriers in the scale [15,47]. Figure 4 shows the kinetic curve of the increase in mass during the oxidation of Fe45Cr0.32Y at 1400°C (curve 1). Heating was carried out at a rate of 35°C/min. The lower section of curve 1 corresponds to heating the sample from room- to operating temperature.

To describe the process under consideration, equation (9) must be solved with the boundary conditions t=0, m=m_0 (or, which is the same, t=t_0, m=0). This solution is:

$$t=2(k^2k_p)^{-1}[e^{km}(km-1)-e^{km_0}(km_0-1)]+(kk_r)^{-1}(e^{km}-e^{km_0}). \quad (18)$$

Time shift between (9) and (18) is:

$$t_0=2(k^2k_p)^{-1}[e^{km_0}(1-km_0)-1]+ (kk_r)^{-1}(1-e^{km_0}). \quad (19)$$

Empirical expression of Eq.(19): $t=843.313[e^{0.022m}(0.022m-1)-0.999]+14.205(e^{0.022m}-1.018)$ (m - in mg/cm², t - in hours), $m_0\cong0.83$ mg/cm², and $t_0\cong-0.43$ h. For comparison, we point out that $m_0=-\bar{m}=k_p/2k_r\cong0.77$ mg/cm².

2.4. Formal kinetics of growth of scale with the increase of the reaction area

Kinetic models of the oxidation processes of alloys could be considered as simplified diagrams of the ambient conditions in which they are located. In the case when are formed easily permeable phases that serve as arteries for diffusion mass transfer, the scale growth kinetic equation can be derived by analogy with the Eq.(5):

$$S/S_0=e^{Km}, \quad (20)$$

where S and S_o are the current and initial values of the effective reaction area, respectively, and K is the constant of the incyrase of the reaction surface. Wherein $S>S_o$.

By analogy of Eqs(9), (10) and (12) we will have:

$$dm/dt=k_p e^{Km} [2m+(k_p/k_r)], \quad (21)$$

$$t=2(K^2k_p)^{-1}[1-e^{-Km}(Km+1)]+(Kk_r)^{-1}(1-e^{-Km}), \quad (22)$$

$$t=2(K^2k_p)^{-1}[1- \Phi\ln(e/\Phi)]+(Kk_r)^{-1}(1- \Phi), \quad (23)$$

where $\Phi=\varphi^{-1}= S_o/S$. Graphs of Eqs(22) and (23) are shown in Fig.5.

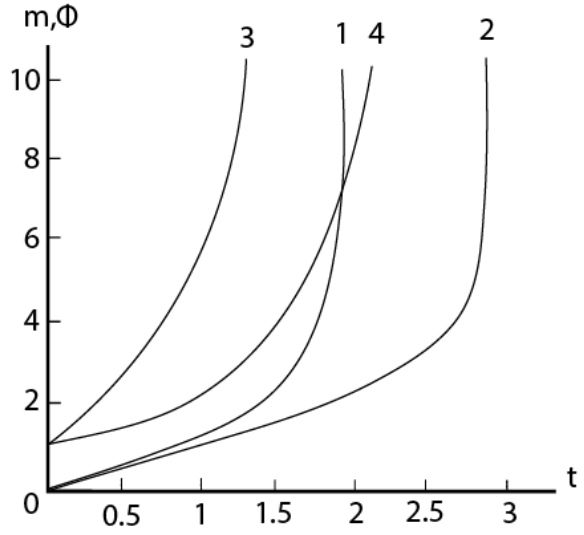

Figure 5. Graphs of Eqs(22) – 1,2 and (23) -3,4; $k_r=\infty$ (1,3), 1(2,4). (K=kp=1.) .

Kinetic curves of a similar shape are presented in a number of works for chromium, nickel-based and other alloys or metals [52-62]. However, it should be noted that purely parabolic kinetics are considered here. Such curves were also obtained during nitriding of germanium powder, where

 doi:10.20944/preprints202309.1173.v1

the metal grains are crushed and, therefore, the reaction surface increases [63]. Prout-Tompkins kinetic model [64] is used here.

Conclusions

The study of the oxidation processes of alloys FeAlCr(La) and FeCr(La) in air at 1300℃ shows the deviation of the oxidation kinetics from parabolic.This is due to the presence of diffusion barriers from chromite $LaCrO_3$ in the scale. This leads to a decrease of the reaction surface for the formation of the basic oxide (Al_2O_3 or Cr_2O_3). When oxidizing a chromia-forming alloy, another secondary process is added - evaporation of Cr_2O_3. Therefore, the equations describing the kinetics of changes in mass of the alloys under study are different.

Equations are considered that make it possible to describe the kinetics of the process taking into account the initial non-isothermal heating. The oxidation process of FeCr(Y) alloy is presented for demonstration.

Formal equations for processes with an increase in the reaction surface are also considered.

Conflicts of Interest: The authors declare no conflict of interest.

References

1. Sharp,W.H. High temperature alloys for the gas turbine - The state of the art**.** *SAE Transactions* **1966**, *74*, 323-332.
2. Klopp,W.D. Recent developments in chromium and chromium alloys. *JOM* **1969**, *21*, 23-32.
3. Bell,S.; Sarvghad,M.; Ong,T.-Ch. et al. Corrosion of iron–nickel–chromium alloys in high temperature carbonate salt under argon atmosphere. *Solar Energy Materials and Solar Cells* 2023, *256*, 112317.
4. Ma,K.; Blackburn,T.; Magnussen,J.P.; Kerbstadt,M. Chromium-based bcc-superalloys strengthened by iron supplements. *Acta Materialia* 2023, *257*, 119183.
5. Li,Z.; Zhao,W.; Zhang,D. et al. Influence of rare-earth element doping on interface and mechanical properties of WC particles reinforced steel matrix composites. *Mater. Res.Express* 2021, 8, 036512.
6. 6.. Othman,N.K.; Jalar,A.; Young,D. Effects of lanthanum on Fe-25Cr alloys under cyclic oxidation. *Adv. Materials Res.* 2010, *97*, 1212-1215.
7. Shi,Z; Chao,W.; Rao,L. et al. Effects of Ce doping on mechanical properties of M7C3 carbides in hypereutectic Fe–Cr–C hardfacing alloy. *Alloys and Comp*. 2021, *850*, 156656.
8. Wu,Z.;G.Wen,G.; Han,Y. Grain growth and oxidation resistance of Fe-Cr-Al electrothermal alloy doped with yttrium. *Ann. Chimie – Sci. des Matériaux* **2020**, *44*, 29-36.
9. Liu,Y.; Chabane,D.; El Kedim,O. First principles investigation of the substitutional doping of rare-earth elements and Co in La4MgNi19 phase. *Energy Stor*. 2023, *67*, 107638.
10. Qin,Y.; Yuan,J.; Zhuang,Y. et al. Study on effect of high-entropy alloy binder on microstructure and properties of WC cemented carbide doped with rare earth *oxide. Coatings* **2023**, *13*, 273 (1-12).
11. Milyutin,V.A.; Birčáková,Z.; Fáberová ,M.; Bures,R. Effect of rare-earth doping on dynamic magnetic properties of FeGa alloy. *Materials Sci. Forum* 2023, *1081*, 149-154.
12. Wang,R.; Tian,X.; Yao,Z. Influence of rare earth element terbium doping on microstructure and magnetostrictive properties of Fe81Al19 alloy. *Rare Earth* 2020, *40*, 451-456.
13. Tian,X.; Zhang,K.; Tan,Ch.; Guo,E. Influence of doping Tb on the mechanical properties and martensitic transformation of Ni-Mn-Sn magnetic shape memory alloys. *Crystals* 2018, *8*, 247.
14. Evans,U.R**.** An introduction to metallic corrosion. London **1981**, 302.
15. Nakhutsrishvili,I.; Mikadze,G. On high-temperature oxidation of alloy FeCr(La): Reduction of the effective diffusion area. *Bull. Georg. Acad. Sci*. **2023**, *17*, 57-63.
16. Mikadze,O.; Kandelaki,A.; Nakhutsrishvili,I. On the kinetics of scale growth with the change of the effective area of diffusion. *Bull. Georgian Acad. Sci*. **2011,** *5*, 73-75.
17. Nakhutsrishvili,I.; Tkeshelashvili,O.; Chanishvili,A. Mathematical model of thermogravimetric curves of FeCrAl(La) alloy. *Technical Sci. & Technologies* **2016**, *5*, 35-37.
18. Xi,Sh.; An,G.; Zhang,X. et al. Corrosion resistance of FeCrAl coatings on Mo–La alloys. *Chinese Mech. Eng. Soc.* **2023**, *41*, 90-96.

19. Wang,I.; Wang,B.;Luo,L. et al. Effects of process atmosphere on additively manufactured FeCrAl oxide dispersion strengthened steel: Printability, microstructure and tensile properties. *Materials Sci. and Eng. A* 2023, *882*,145438.
20. Wang,I.; Binbin Wang,B.; Liangshun Luo,L. et al. Effects of process atmosphere on additively manufactured FeCrAl oxide dispersion strengthened steel: Printability, microstructure and tensile properties. *Materials Sci. and Eng. A* 2023, 882,145438.
21. Hoelzer,D.T.; Heidel,D.; Yamamoto,Y.; Massey,C.P. High-Temperature creep behavior of thin-walled FeCrAl alloy tubes. Oak Ridge National Lab. **2023**, ORNL/LTR-2023/2888.
22. Jiang,H.; Zhao,X.; Wang,D. et al. Effects of Y_2O_3 addition on the microstructure and static lead-bismuth eutectic thermal corrosion behaviors of FeCrAlTiC-xY_2O_3lLaser clade coatings. *Coatings* 2022,*12*,1759.
23. Saito,Y. Effect of rare earth elements on the high-temperature oxidation of heat-resisting alloys. In: Selected topics in high-temperature chemistry **1989**, Amsterdam-Oxford-New-York-Tokyo: Elsevier, 227.
24. Ishii, K.; Kohno, M.; Ishikawa, S.,;Satoh, S. Effect of rare-earth elements on high-temperature oxidation resistance of Fe-20Cr-5Al alloy foils. *Materials Transact.* **2011**, *38*, 787-792.
25. Hou, P.Y. The reactive element effect – Past, present and future. *Materials Sci. Forum* **2011**, *696*, 39-44.
26. Ozawa, M., Araki, K.-I. Effect of La modification on the stability of coating alumina layer on FeCrAl alloy substrate. *Surf. and Coatings Technology* **2015**, *271*, 80-86.
27. He, Y.; Liu, J.H.; Han, Z.B. et al. Effect of La on mechanical Properties of FeCrAl stainlees steel under high temperature. *Contin. Casting* **2015**, 40, 1-9.
28. Nakatsuka, A.; Ohtaka, O.; Arima, H. et al.(2005). Cubic phase of single-crystal $LaAlO_3$ perovskite synthesized at 4.5 GPa and 1273 K. *Acta Crystallog.* **2005**, *E61*, i148-i150.
29. Boudali, A.; Saadaoui, F.; Zemouli, M. et al. Recalculate structural, elastic, electronic and thermal properties in $LaAlO_3$ rhombohedral perovskites. *Adv. in Materials Phys. and Chem.* **2013**, *3*, 146-152.
30. Liu,Z.; Gao,; He Y. Modeling of oxidation kinetics of Y-doped Fe-Cr-Al alloys. *Oxidat. Metals* **2000**, *53*, 341-350.
31. Badini,C.; Laurella,F. Oxidation of FeCrAl alloy: Influence of temperature and atmosphere on scale growth rate and mechanism. *Surface and Coatings Technol*. **2001**, *135*, 291-298.
32. Zhang,Z.G.; Gesmundo,F.; Hou,P.Y.; Niu,Y. Criteria for the formation of protective Al_2O_3 scales on Fe-10Al and FeCrAl alloys. *Corrosion Sci.* **2006**, *48*, 741-765.
33. Young,D.J.; Niewalak,L.; Wessel,E. et al. Oxidation kinetics of Y-doped FeCrAl alloys in low and high PO_2 gases. *Materials and Corros.* **2010**, *61*, 838-844.
34. Othman,N.K.; Zhang,J.; Young,D.J. Water vapour effects on Fe-Cr alloy oxidation. *Oxidat.* Metals **2010**, *73*, 337-352.
35. Tallman,D.J.; Anasori,B.; BarsoumM.W. A critical review of the oxidation of Ti_2AlC, $Ti3AlC_2$ and Cr_2AlC in air. *Materials Res. Lett*. **2013**, *1*, 115-125.
36. Hellström,K.; Israelsson,;N., Mortazavi,N. et al. Oxidation of a dispersion-strengthened powder metallurgical FeCrAl alloy in the presence of O_2 at 1,100°C: the influence of water vapour. *Oxidat. Metals* **2015**, *83*, 533-558.
37. Quadakkers,W.J.; Wessel,E.; Kochubey, V. et al. Growth rates of alumina scales on Fe-Cr-Al alloys. *Oxidat. Metals* **2004**, *61*, 17-37.
38. Chegroune,R.; Salhi,E.; Gri**sci**,A. et al. High-temperature corrosion of dilute chromium-lanthanum alloys. *Oxidat. Metals*, **2008**, *70*, 331-350.
39. Taniguchi,S.; Andoh,A. Improvement in the oxidation resistance of an Al-deposited Fe–Cr–Al foil by preoxidation. *Oxidat. Metals* 2022, *58*, 545-562.
40. Wolff,M.; EIorio,L.; Rumpf,T. Oxidation and corrosion behaviour of Fe–Cr and Fe–Cr–Al alloys with minor alloying additions. *Materials Sci. Eng. A* 1998, *241*, 264-276.
41. Pint,B.A. Optimization of reactive-element additions to improve oxidation performance of alumina-forming alloys. *Amer. Ceramic. Soc*. 2003, *86*, 686-695.
42. du Prees,S.P.; van Kaam,T.P.M.; Ringdalen,E. et al. An Overview of currently applied ferrochrome production processes and their waste management practices. *Minerals* 2023, *13*, 809.
43. Wang,W.; Pan,Q.; Wang,X. et al. Non-isothermal aging: A heat treatment method that simultaneously improves the mechanical properties and corrosion resistance of ultra-high strength Al-Zn-Mg-Cu alloy. *Alloys and Comp*. **2020,** *845*, 156286.

44. Sharma,P.; Kainth,S.; Singh,K. et al. Investigating non-isothermal oxidation kinetics of a non-stoichiometrically synthesized Ti_3AlC_2 MAX phase. *Alloys and Comp*. **2023**, *959*,170488.
45. Yang,J.; Liu,H.; Zeng,T. et al. Effect of non-isothermal aging on the mechanical properties and corrosion resistance of 2A12 aluminum alloy. *Materials* **2023**, *16*, 3921.
46. Ouyang,P,; Mi,G.; Li,P.et al. Non-isothermal oxidation behaviors and mechanisms of Ti-Al intermetallic compounds. *Materials* **2019**, *12*, 2114.
47. Nakhutsrishvili,I.; Mikadze,G.; Mikadze,O. Mutual connection of unisothermal initial heating with isothermal oxidation kinetics of heat resistant chromium alloys. *Proc. Georgian Acad. Sci., chem. ser.* 2007, *33*, 60-63.
48. Pillis,M.F.; Correa, O.V.; Ramanathan,L.V. High-temperature corrosion behavior of yttrium dioxide coated Fe-20Cr Alloy. *Materials Res.* **2016**, *19*, 611-617.
49. Fontana,S; Vuksa,M et al. On the effect of surface treatment to improve oxidation resistance and conductivity of metallic interconnects for SOFC in operating conditions. *Mater. Sci. Forum* **2008**, *595/598*, 753-762.
50. Sayto Y, Önay B, Maruyama T. The Reactive Element Effect (REE) in oxidation of alloys Phys. IV Fr. 1993;3:C217-C230.
51. Molin S, Persson AH, et al. Effective yttrium based coating for steel interconnects of solid oxide cells: Corrosion evaluation in steam-hydrogen atmosphere. power sources. 2019;440:article id.26814.
52. Yoneda,S; Hayashi,S.; Ukai,S. The transition from transient oxide to protective Al_2O_3 scale on Fe–Cr–Al alloys during heating to 1000°C. *Oxidat. Met*. 2018, *89*, 81-97.
53. Pillis,M.F.; Ramanathan,L.V. Effect of pre-oxidation on high temperature sulfidation behavior of FeCr and FeCrAl alloys. *Materials Res*. **2004**, *7*, 97-102.
54. Gheno,T.; Monceau,D.; Young,D.J. Kinetics of breakaway oxidation of Fe–Cr and Fe–Cr–Ni alloys in dry and wet carbon dioxide. *Corrosion Science* 2013, *77*, 246-256.
55. Wright,I.G.; Peraldt,R. Oxidation-limited lifetime of ODS-FeCrAl alloys: Observations on influence of surface shape. *High Temp. Corrosion of Materials* 2023, *99*, 183–200.
56. Ma,S.; Ding,Q.; Wei,X. et al. The effects of alloying elements Cr, Al, and Si on oxidation behaviors of Ni-based superalloys. *Materials* 2022, *15*, 7352.
57. Jönsson,B.; Westerlund, A. Oxidation comparison of alumina-forming and chromia-forming commercial alloys at 1100 and 1200°C. *Oxidat. Met.* 2017; *88*: 315-326.
58. Cheng,Ch.; Li,X.; Le,Q. et al. Effect of REs (Y, Nd) addition on high temperature oxidation kinetics, oxide layer characteristic and activation energy of AZ80 alloy. *Magnesium and Alloys* **2020**, *8*, 1281-1295.
59. Zemlyanov,D.; Klötzer,B.; Gabasch,H. et al. Kinetics of palladium oxidation in the mbar pressure range: Ambient pressure XPS study. *Topics Catal.* 2013, *56*, 885–895.
60. Gasparini,C.; Chater,R.J.; Horlait,D. et al. Zirconium carbide oxidation: Kinetics and oxygen diffusion through the intermediate layer *Amer. Ceramic Soc.* **2018**, *101*, 2638-2652.
61. Lo,K.-Ch.; Chang,Y.-J.; Murakami,H. et al.An oxidation resistant refractory high entropy alloy protected by $CrTaO_4$-based oxide. *Sci. Pep*. 2019, *9*,7266.
62. Motta,A.T.; Gomes da Silva,M.J.;Yilmazbayhan,A. et al. Microstructural characterization of oxides formed on model Zr alloys using synchrotron radiation. *ASTM Intern*. 2008, *5*, JAI101257.
63. Labbe,J.-C.; Duchez,F.; Billy,M. Nitruration du germanium pulvérulent par l'ammoniac.*Compt. Rend. Acad. Sci. Paris* **1971**, *273*, 1750-1753.
64. Brown,M.E. The Prout-Tompkins rate equation in solid-state kinetics. *Thermochim. Acta* 1997, *300*, 93-106.